

Extension of the QuikSCAT Sea Ice Extent Data Set With OSCAT Data

Jordan C. Hill and David G. Long, *Fellow, IEEE*

Abstract—The Ku-band Oceansat-2 Scatterometer (OSCAT) is very similar to the Quick Scatterometer (QuikSCAT), which operated from 1999 to 2009. OSCAT continues the Ku-band scatterometer data record through 2014 with an overlap of 19 days with QuikSCAT’s mission in 2009. This letter discusses a particular climate application of the time series for sea ice extent observation. In this letter, a QuikSCAT sea ice extent algorithm is modified for OSCAT. Gaps in OSCAT data are accounted for and filled in to support sea ice extent mapping. The OSCAT sea ice extent data are validated with QuikSCAT and Special Sensor Microwave/Imager sea ice extent data.

Index Terms—Arctic, Antarctic, radar remote sensing, sea ice.

I. INTRODUCTION

SPACEBORNE wind scatterometers are primarily designed to measure wind speeds over the ocean. Scatterometers measure the normalized radar cross section (σ^0) of the surface [1]. This σ^0 backscatter measurement provides useful data for other scientific land and ice applications [2]–[7]. One such application is the measurement of sea ice extent in the polar regions. Ku-band scatterometers are well suited for mapping the sea ice extent because of the high contrast between σ^0 measurements of the ocean compared with sea ice.

An algorithm was developed to map the daily sea ice extent, in both the Arctic and Antarctic regions, from σ^0 measurements for the Ku-band NASA Scatterometer (NSCAT) [1] and for the Ku-band SeaWinds instrument aboard the Quick Scatterometer (QuikSCAT) [8]. In order to continue the scatterometer sea ice extent data set, the algorithm is adapted and applied to the Ku-band Oceansat-2 Scatterometer (OSCAT) [9]. This letter discusses these adjustments and validates the OSCAT ice extent data set with QuikSCAT and Special Sensor Microwave/Imager (SSM/I) data sets.

II. BACKGROUND

Polar sea ice plays an important role in climate [10]. The NSCAT algorithm for sea ice mapping [11] was developed by Remund and Long [12] and later adapted for QuikSCAT. It uses an iterative maximum-likelihood classifier with fixed thresholds to classify sea ice pixels from QuikSCAT scatterometer image reconstruction (SIR) images [13].

Manuscript received March 9, 2016; revised August 15, 2016; accepted November 14, 2016. Date of publication December 8, 2016; date of current version December 26, 2016.s

The authors are with the Electrical and Computer Engineering Department, Brigham Young University, Provo, UT 84602 USA (e-mail: hill@mers.byu.edu; long@ee.byu.edu).

Color versions of one or more of the figures in this letter are available online at <http://ieeexplore.ieee.org>.

Digital Object Identifier 10.1109/LGRS.2016.2630010

The QuikSCAT wind mission ended in 2009, but the continuation of the Ku-band scatterometer data climate record is made possible through the operation of OSCAT, which began its data collection 18 days before the end of QuikSCAT’s wind mission. OSCAT operates with the same pencil-beam design as QuikSCAT. The similarity enables the QuikSCAT sea ice extent algorithm to be applied to OSCAT data. However, data gaps persist in the OSCAT data set. To address this problem, the OSCAT sea ice extent algorithm is modified from the QuikSCAT algorithm to account for the gaps in the OSCAT data set.

III. MULTIVARIATE SEA ICE EXTENT MAPPING

The QuikSCAT sea ice extent algorithm is summarized briefly here and is found in more detail in [12]. For each daily image pixel, four parameters are combined into a 4-D feature vector. These parameters are: 1) a modified copol ratio, which is the ratio of the vertical polarization (v-pol) σ^0 at 54° incidence angle to the horizontal polarization (h-pol) σ^0 at 46° incidence angle and the 2) h-pol σ^0 , and the standard deviations of the 3) v-pol and 4) h-pol σ^0 estimate error. The parameters are each normalized to a mean of zero and a variance of one. Remund and Long [12] found that sea ice detection performance is better when the copol ratio is weighted in importance four times more than the other three parameters when generating the histogram. A daily 4-D histogram is computed to estimate a bimodal sea ice/ocean joint distribution for that day.

A linear discrimination technique is first applied for classification. An automated 4-D histogram search algorithm locates the saddle point on the transect connecting the ocean and sea ice peaks. A line orthogonal to the transect is drawn through the saddle point and the pixels are then classified as ocean or sea ice based on which side of the line they fall on. This initial classification is improved with an iterative maximum-likelihood classification technique adopted from [14]. A region growing technique [11] is then applied to eliminate residual patches of ocean misclassified as sea ice and vice versa.

Because of misclassified “extrusions” or “indentations” in the ice edge that persist following the classification procedure, the final step of the algorithm is sea ice growth/retreat constraint filtering. Image dilation and erosion techniques [15], [16] combine the previous day’s sea ice extent σ^0 backscatter image with a threshold of 200-km maximum edge motion per day [12]. Following erosion, disconnected extrusions on the ice edge are reclassified as water; following dilation, filled indentations are reclassified as ice.

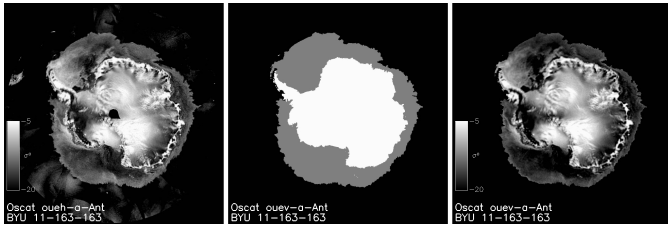


Fig. 1. Images from the sea ice mask processing stages for day 163 of 2011. The left image is the h-pol σ^0 at 46° incidence angle used as one of the 4-D feature vector parameters applied to the image. The center image is the final trinary sea ice mask. The right image is the final processed σ^0 sea ice mask.

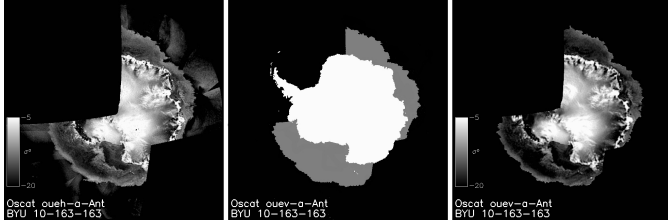


Fig. 2. Images from the sea ice mask processing stages for day 163 of 2010 illustrating the processing of images with missing data. Like in Fig. 1, the left image is the h-pol σ^0 at 46° incidence angle used as one of the 4-D feature vector parameters applied to the image. The center image is the final trinary sea ice mask. The right image is the final processed σ^0 sea ice mask.

The result is a trinary mask with different values assigned to water, ice, and land. Example images are shown in Fig. 4.

IV. OSCAT ADJUSTMENTS

OSCAT had known mounting issues and a small latitude-dependent bias. However, in the polar regions, the bias is relatively small and thus is ignored in the ice mapping processing. A small calibration offset in σ^0 between OSCAT and QuikSCAT exists. However, the water/ice threshold used in the sea ice extent algorithm is set dynamically so the bias has no impact on the algorithm performance or the resulting ice masks.

Available data for OSCAT, obtained as LIB OSCAT V1.1 data processed by the Indian Space Research Organization and obtained from the European Organization for the Exploitation of Meteorological Satellites via the National Oceanic and Atmospheric Administration, ranges from day 309 of year 2009 to day 51 in year 2014. Daily OSCAT SIR images are processed into sea ice maps using the modified QuikSCAT ice mapping algorithm. Most days are processed normally as shown in Fig. 1. The various parameters, such as the h-pol σ^0 backscatter image shown on the left, are run through the algorithm after being normalized to a mean of zero and a variance of one. The resulting masked σ^0 backscatter image is shown on the right. Due to data dropouts, however, missing data are prevalent in a number of days during OSCAT's mission. This is shown in Fig. 2. The algorithm classifies the data available as shown in the middle and right images of Fig. 2, but portions corresponding to missing data remain blank. The consequence of this missing data arises when using this sea ice extent image to constrain allowable sea ice movement for the next day.

The QuikSCAT sea ice mask algorithm uses the σ^0 backscatter ice mask as the previous day's constraint mask. This works exceptionally well with QuikSCAT, because the data are continuous. Modifications are applied to the OSCAT sea ice extent algorithm to overcome the coverage inconsistency in data for OSCAT. Fig. 3 shows a sample of OSCAT σ^0 ice mask images with missing data from four different days of OSCAT's mission, including the finished SIR ice mask sample of day 163 from 2010. The missing data limits the utility of these σ^0 backscatter sea ice masks for use as the previous day constraint for the following day's mask.

To compensate for this issue, the missing data for the trinary mask are filled in with the previous day's trinary mask. The data gaps shown in Fig. 3 are filled in using data from the trinary ice masks of the previous day as shown in Fig. 4. With this correction, OSCAT sea ice extent images are processed using the trinary image as the previous day's constraint rather than the σ^0 backscatter sea ice extent image, which is used for the QuikSCAT algorithm. By doing so, sea ice extent maps from days with partially missing data are filled in properly with correct data and the resulting OSCAT sea ice extent data set is more consistent.

A. Reverse Processing Approach

This simple procedure does not, however, correct all sea ice extent problems that arise from consecutive days of missing data in the OSCAT data set. One such stretch of days for OSCAT occurs from day 182 to day 273 in 2010. Due to power fluctuations [17], σ^0 data during that time are incorrect, and therefore, images over this period are not processed. The lack of data causes a problem when attempting to process the sea ice extent map for day 274. The nearest sea ice extent map available for use as the previous day constraint mask comes from day 181. Using day 181 as the constraint mask for day 274 would inaccurately constrain the sea ice growth for day 274.

To address this problem, a reverse time processing approach is used when long gaps occur. Rather than using the previous day as the constraint mask, the current day is used as the constraint mask for the previous day. With this approach, the trinary mask for day 278 of 2010 is used as the constraint for day 277 while day 277 is reprocessed. The new trinary mask from day 277 is then used as the constraint for day 276 and so on until day 274 is reprocessed with a more accurate constraint mask based on the future.

The reprocessed sea ice mask of day 274 is a much better representation of the actual sea ice extent compared with the first processed mask as shown in Fig. 5. The results of the forward processing technique are represented by the dotted-dashed line, and the reverse processing technique is represented by the dashed line. For comparison, the previous three years of QuikSCAT sea ice extent data for these days are represented by the solid lines. The reverse processing technique follows the ice extent trends of previous years better than the forward processing technique. The forward processing technique requires two to three days to catch up. This supports the use of the reverse processing technique following large gaps in the data. The noncausal reverse

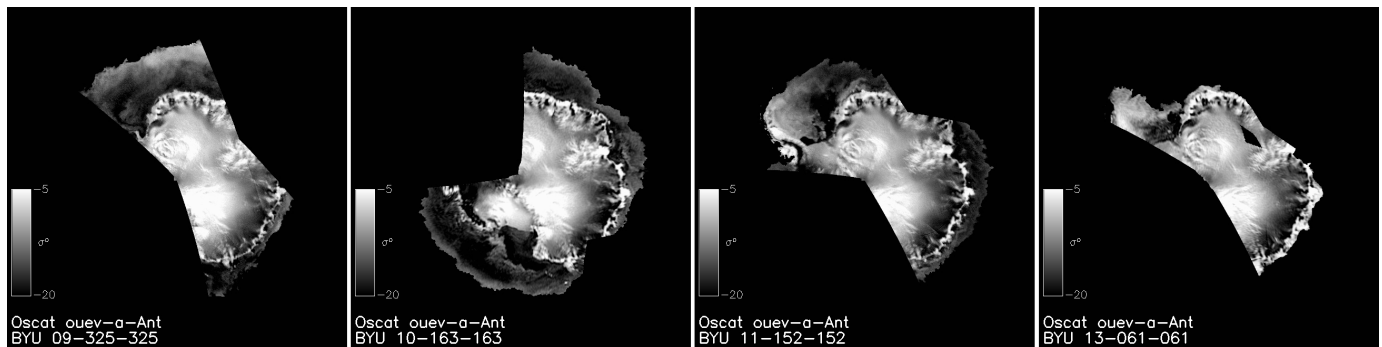


Fig. 3. Sample of OSCAT SIR ice-masked images. Each of the four images has missing data due to data downlink problems.

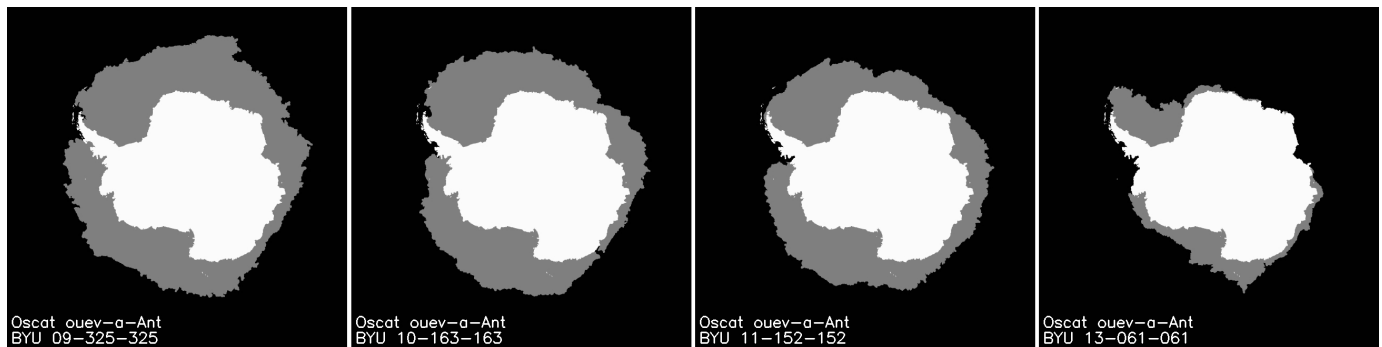


Fig. 4. Trinary OSCAT ice extent products corresponding to the four SIR images in Fig. 3. The trinary ice mask from the previous day is used to fill in the data gaps from the SIR images.

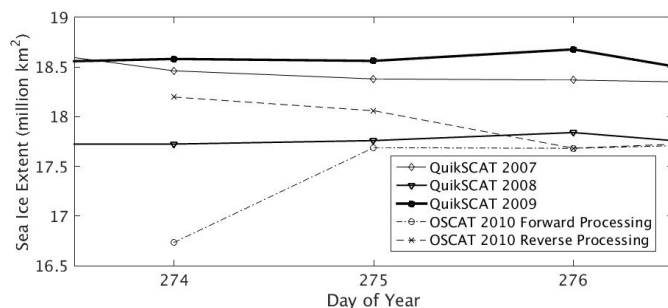


Fig. 5. Comparison of the forward and reverse processing techniques in total sea ice extent during days 274, 275, and 276 in 2010 in Antarctica, with QuikSCAT total sea ice extent data over the same days from 2007 to 2009. This sea ice extent data are processed after the long data gap in 2010.

processing approach is used to correct for data gaps of two days or more.

Fortunately, the 2010 data gap is the only gap longer than 15 days, though there is another data gap of 15 days in 2012. Other data gaps are five days or less. Because these data gaps happen randomly throughout the data set and the gaps make up only 10% of the potential OSCAT data set, OSCAT yearly trends and means are not negatively affected by the data gaps.

V. RESULTS

The modified sea ice extent algorithm is applied to the entire OSCAT mission. Coupled with the QuikSCAT data set, this provides a nearly continuous sea ice extent data set for the polar regions from 1999 to 2014. The OSCAT sea ice extent is validated using the overlapping period with QuikSCAT and the NASA Team algorithm applied to SSM/I.

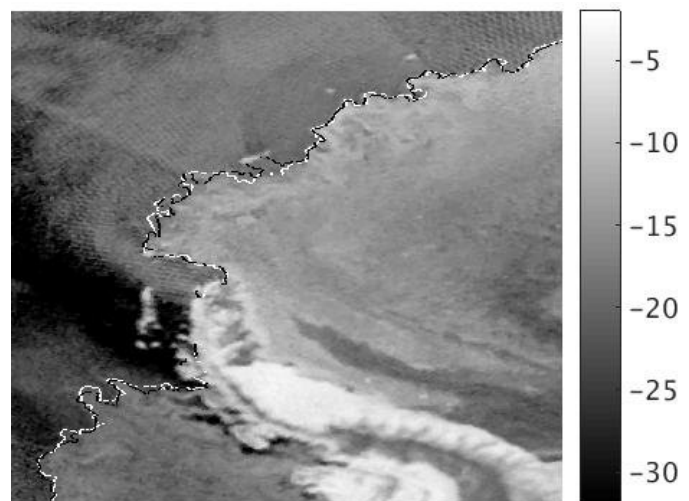


Fig. 6. Sea ice edge comparison in the Weddell Sea region of Antarctica showing the QuikSCAT ice edge (white line) and the OSCAT ice edge (black line). The background image is the OSCAT σ^0 image from day 319 of 2009. White areas left of the ice edge are islands and icebergs that are not included in the ice mask.

A. QuikSCAT Comparison

QuikSCAT and OSCAT overlap from day 309 to day 327 in 2009. Due to three days of missing OSCAT data during this span, there are 16 days of data that overlap between the instruments. The two data sets are compared during this overlap period. Fig. 6 shows a QuikSCAT slice SIR image of the Weddell Sea from day 319 of 2009. The derived ice edges from QuikSCAT and OSCAT are superimposed on the

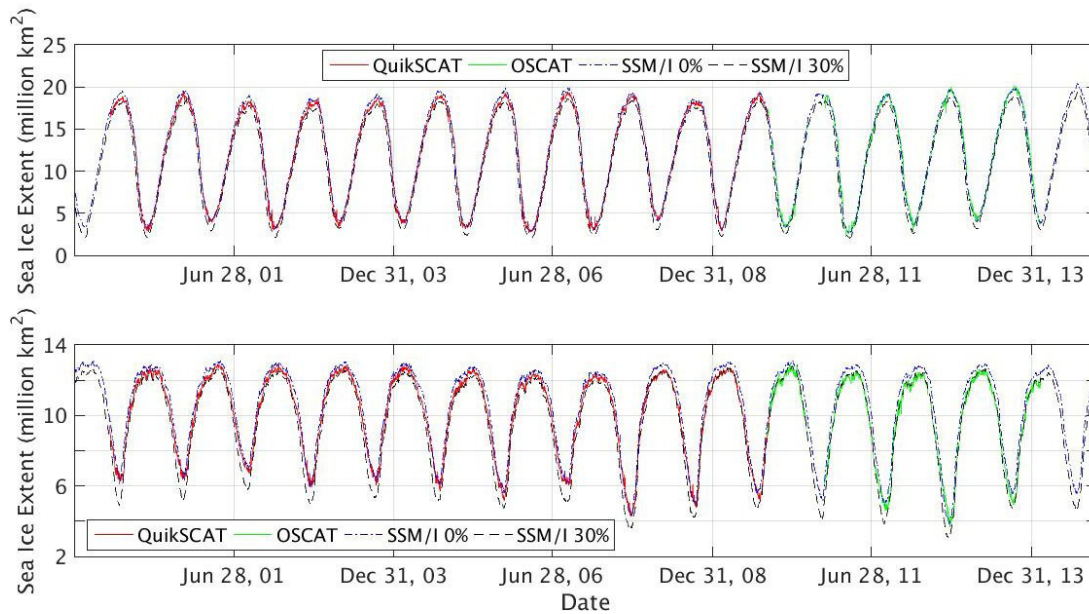


Fig. 7. Sea ice extent over the lifetime of QuikSCAT (red) and OSCAT (green) in the (top) Antarctic and the (bottom) Arctic above 60° latitude. The data from the two instruments are compared with the SSM/I 0% and 30% sea ice extents.

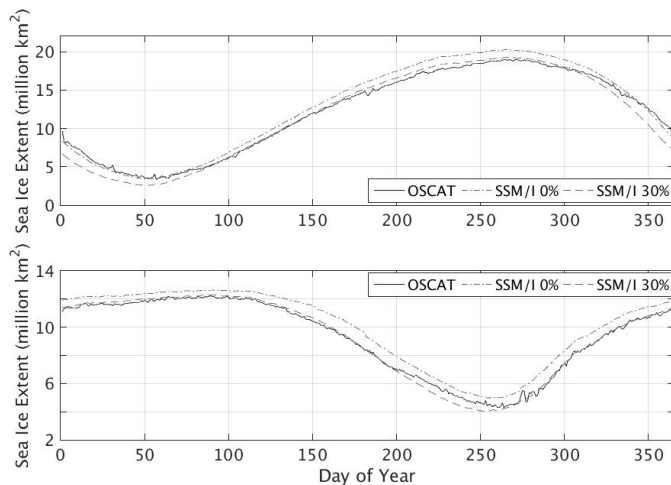


Fig. 8. Mean daily (top) Antarctic and (bottom) Arctic sea ice total extent from 2009 to 2014. The OSCAT extent is compared with SSM/I 0% and 30% mean sea ice extent.

QuikSCAT SIR image from 2009. Note the close correlation between the ice masks of the two sensors. Note also the icebergs at the top of the image, which are correctly removed from the overall sea ice extent. The Antarctic Peninsula and the South Shetland Islands, prominently shown in Fig. 6, are masked out of the algorithm processing and are therefore not included in the sea ice extent. It may be that the darker splotches along the lower coast of the Antarctic Peninsula are polynyas, areas of open water surrounded by ice. While these are technically not areas of sea ice, they are included in the sea ice extent as being inside the larger boundary between sea ice and ocean.

The root-mean-square error between the sea ice extents measured by the two instruments over the 16 overlapping days is 0.12 million km^2 for the Antarctic region and 0.24 million km^2 for the Arctic region. From the QuikSCAT and OSCAT comparisons, we conclude that the OSCAT

modified sea ice extent algorithm reasonably matches the QuikSCAT ice extent data set during the overlapping period in both the Arctic and Antarctic regions.

B. NASA Team Algorithm Comparison

The OSCAT data set daily measurements of total sea ice area are compared with SSM/I sea ice extent data. SSM/I sea ice classification is from the NASA Team algorithm [18]. This algorithm classifies ice based on multifrequency dual-polarization data from the passive radiometer, SSM/I. This data are retrieved from the national snow and ice data center [19].

OSCAT pixels flagged as ice are summed for each day and a total area is computed using the 4.5-km pixel size of the polar stereographic projection. SSM/I-generated sea ice extent map pixels are on a 25-km polar stereographic projection grid. The NASA Team algorithm produces various percent ice concentrations that are used for comparison. Total sea ice extent for different concentrations is calculated by summing only pixels above the concentration threshold.

The OSCAT daily sea ice extent results for the two polar regions from 2009 to 2014 are shown in Fig. 7. The QuikSCAT daily sea ice extent results for its mission life from 1999 to 2009 are included to create a continuous time-series of data. The SSM/I-measured 0% and 30% ice concentration extent values are given for comparison. The OSCAT- and QuikSCAT-measured sea ice extents in the Arctic are calculated only from sea ice above 60° latitude to align with SSM/I sea ice extent data. Despite some inconsistency in OSCAT data, it is seen in Fig. 7 that OSCAT-measured sea ice extent generally falls between the SSM/I 0% and 30% measured sea ice extent, which is consistent with QuikSCAT performance [12]. This consistency is also shown in the sea ice extent differences between the different instruments shown in Fig. 9. The OSCAT data shows similar trends to QuikSCAT data.

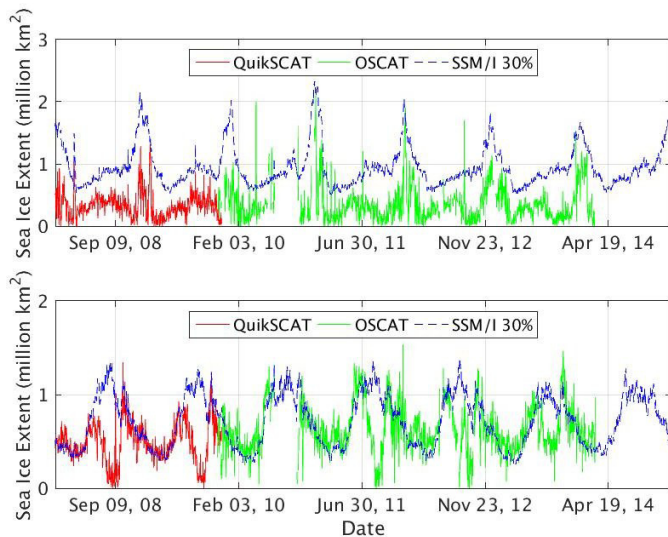


Fig. 9. Sea ice extent differences with SSM/I 30% data in the (top) Antarctic and the (bottom) Arctic. QuikSCAT, shown in red, concludes at the end of 2009. OSCAT, shown in green, begins right at the end of QuikSCAT and continues to the beginning of 2014.

Daily means of the sea ice extent of both the Antarctic and Arctic regions over the life of OSCAT are shown in Fig. 8. Both are shown in comparison with SSM/I 0% and 30% daily mean sea ice extents. The Antarctic extent in particular shows that the OSCAT sea ice extent correlates to the SSM/I 0% ice concentration during the austral summer and to the SSM/I 30% ice concentration during the austral winter. The differences may be caused by a different frequency use, passive versus active microwave measurements, different polarizations, algorithm methods, and so on. A deeper exploration of these differences is found in [12] and [20].

VI. CONCLUSION

The QuikSCAT ice edge algorithm has proved useful for the QuikSCAT data set [12]. Noncausal processing of OSCAT data using that algorithm creates an ice extent data set that continues where QuikSCAT left off. The OSCAT data set is validated using the SSM/I-derived NASA Team algorithm 0%–30% ice extents.

The QuikSCAT and OSCAT data sets are combined to provide a continuous data set of Ku-band scatterometer-derived sea ice extents from 1999 to 2014. This data set is publicly available from the Scatterometer Climate Record Pathfinder (www.scp.byu.edu). Further extension of the data set using additional scatterometers is being explored.

REFERENCES

- [1] F. M. Naderi, M. H. Freilich, and D. G. Long, "Spaceborne radar measurement of wind velocity over the ocean—an overview of the NSCAT scatterometer system," *Proc. IEEE*, vol. 79, no. 6, pp. 850–866, Jun. 1991.
- [2] D. G. Long and M. R. Drinkwater, "Greenland ice-sheet surface properties observed by the Seasat-A scatterometer at enhanced resolution," *J. Glaciol.*, vol. 40, no. 135, pp. 213–230, 1994.
- [3] S. H. Yueh, R. Kwok, S.-H. Lou, and W.-Y. Tsai, "Sea ice identification using dual-polarized Ku-band scatterometer data," *IEEE Trans. Geosci. Remote Sens.*, vol. 35, no. 3, pp. 560–569, May 1997.
- [4] D. G. Long and M. R. Drinkwater, "Cryosphere applications of NSCAT data," *IEEE Trans. Geosci. Remote Sens.*, vol. 37, no. 3, pp. 1671–1684, May 1999.
- [5] S. E. L. Howell, C. Derksen, and A. Tivy, "Development of a water clear of sea ice detection algorithm from enhanced SeaWinds/QuikSCAT and AMSR-E measurements," *Remote Sens. Environ.*, vol. 114, no. 11, pp. 2594–2609, 2010.
- [6] M. B. Rivas and A. Stoffelen, "New Bayesian algorithm for sea ice detection with QuikSCAT," *IEEE Trans. Geosci. Remote Sens.*, vol. 49, no. 6, pp. 1894–1901, Jun. 2011.
- [7] D. B. Lindell and D. G. Long, "Multiyear Arctic sea ice classification using OSCAT and QuikSCAT," *IEEE Trans. Geosci. Remote Sens.*, vol. 54, no. 1, pp. 167–175, 2016, doi: 10.1109/TGRS.2015.2452215.
- [8] M. W. Spencer, C. Wu, and D. G. Long, "Improved resolution backscatter measurements with the SeaWinds pencil-beam scatterometer," *IEEE Trans. Geosci. Remote Sens.*, vol. 38, no. 1, pp. 89–104, Jan. 2000.
- [9] J. P. Bradley and D. G. Long, "Estimation of the OSCAT spatial response function using island targets," *IEEE Trans. Geosci. Remote Sens.*, vol. 52, no. 4, pp. 1924–1934, Apr. 2014.
- [10] W. F. Budd, "Antarctic sea-ice variations from satellite sensing in relation to climate," *J. Glaciol.*, vol. 15, no. 73, pp. 417–427, 1975.
- [11] Q. P. Remund and D. Long, "Sea ice extent mapping using Ku band scatterometer data," *J. Geophys. Res.*, vol. 104, no. C5, pp. 11515–11527, 1999.
- [12] Q. P. Remund and D. G. Long, "A decade of QuikSCAT scatterometer sea ice extent data," *IEEE Trans. Geosci. Remote Sens.*, vol. 52, no. 7, pp. 4281–4290, Jul. 2014.
- [13] D. S. Early and D. G. Long, "Image reconstruction and enhanced resolution imaging from irregular samples," *IEEE Trans. Geosci. Remote Sens.*, vol. 39, no. 2, pp. 291–302, Feb. 2001.
- [14] Q. P. Remund, D. G. Long, and M. R. Drinkwater, "An iterative approach to multisensor sea ice classification," *IEEE Trans. Geosci. Remote Sens.*, vol. 38, no. 4, pp. 1843–1856, Jul. 2000.
- [15] J. C. Russ, *The Image Processing Handbook*. Boca Raton, FL, USA: CRC Press, 2011.
- [16] W. Pratt, *Digital Image Processing*. New York, NY, USA: Wiley, 1991.
- [17] S. A. Bhowmick, R. Kumar, and A. S. K. Kumar, "Cross calibration of the oceanSAT -2 scatterometer with QuikSCAT scatterometer using natural terrestrial targets," *IEEE Trans. Geosci. Remote Sens.*, vol. 52, no. 6, pp. 3393–3398, Jun. 2014.
- [18] D. J. Cavalieri, C. L. Parkinson, P. Gloersen, and H. J. Zwally, "Arctic and Antarctic sea ice concentrations from multichannel passive-microwave satellite data sets: User's guide," NASA, Washington, DC, USA, Tech. Rep. 104647, Oct. 1978.
- [19] D. Cavalieri, C. Parkinson, P. Gloersen, and H. Zwally, "Sea ice concentrations from Nimbus-7 SMMR and DMSP SSM/I-SSMIS passive microwave data. [subset 2009–2014]," NASA, Boulder, CO, USA, Data Set NSIDC-0051, 1996. [Online]. Available: <http://dx.doi.org/10.5067/8GQ8LZQVL0VL>
- [20] W. N. Meier and J. Stroeve, "Comparison of sea-ice extent and ice-edge location estimates from passive microwave and enhanced-resolution scatterometer data," *Ann. Glaciol.*, vol. 48, no. 1, pp. 65–70, Jun. 2008.